International Journal of Biological Macromolecules 213 (2022) 259–267

Contents lists available at ScienceDirect

International Journal of Biological Macromolecules

journal homepage: www.elsevier.com/locate/ijbiomac

Investigation of 3D-printed chitosan-xanthan gum patches

Eray Altan [a], Nurgul Turker [b], Osama Ali Hindy [c], Zeynep Dirican [d], Ozlem Bingol Ozakpinar [e], Aysegul Uzuner Demir [f], Deepak Kalaskar [g,*], Sourbh Thakur [h,i], Oguzhan Gunduz [a,j,**]

[a] Department of Metallurgy and Materials Engineering, Faculty of Technology, Marmara University, Istanbul, Turkey
[b] Department of Bioengineering, Faculty of Engineering, Marmara University, Istanbul, Turkey
[c] Department of Biomedical Engineering, School of Engineering and Natural Sciences, Istanbul Medipol University, Istanbul, Turkey
[d] Eyuboglu College, Istanbul, Turkey
[e] Department of Basic Pharmaceutical Sciences, Faculty of Pharmacy, Marmara University, Istanbul, Turkey
[f] Kazlicesme R&D Center and Test Laboratories, Tuzla, Istanbul, Turkey
[g] UCL Division of Surgery and Interventional Science, Royal Free Hospital Campus, University College London, Rowland Hill Street, NW3 2PF, UK
[h] Department of Organic Chemistry, Bioorganic Chemistry and Biotechnology, Silesian University of Technology, B. Krzywoustego 4, 44-100 Gliwice, Poland
[i] School of Advanced Chemical Sciences, Shoolini University, Solan 173229, Himachal Pradesh, India
[j] Center for Nanotechnology & Biomaterials Application and Research (NBUAM), Marmara University, Istanbul, Turkey

ARTICLE INFO

Keywords:
3D printing
Biomaterials
Wound dressing
Optimisation

ABSTRACT

In this study, using a new polymer combination of Chitosan(CH)/Xanthan Gum(XG) has been exhibited for wound dressing implementation by the 3D-Printing method, which was fabricated due to its biocompatible, biodegradable, improved mechanical strength, low degradation rate, and hydrophilic nature to develop cell-mimicking, cell adhesion, proliferation, and differentiation. Different concentrations of XG were added to the CH solution as 0.25, 0.50, 0.75, 1, and 2 wt% respectively in the formic acid/distilled water (1.5:8.5) solution and rheologically characterized to evaluate their printability. The results demonstrated that high mechanical strength, hydrophilic properties, and slow degradation rate were observed with the presence and increment of XG concentration within the 3D-Printed patches. Moreover, in vitro cell culture research was conducted by seeding NIH 3T3 fibroblast cells on the patches, proving the cell proliferation rate, viability, and adhesion. Finally, 1% XG and 4% CH containing 3D-Printed patches were great potential for wound dressing applications.

1. Introduction

Lately, skin diseases are considered one of the most common causes of all human diseases, affecting around 900 million people worldwide [1]. Skin is an essential natural organ covering the entire body and protecting its internal organs by providing a protective barrier against any external harm from the environment [2]. Hence, the development of a rapid and efficient skin treatment has been the primary concern of modern medical researchers. Chitosan (CH) is an abundant natural polymer with a linear chain with various advantages, including high biocompatibility, antibacterial properties, cationic charge, biodegradability, and hydrophilicity [3]. Besides, several studies have proven that CH can be used to accelerate the wound healing process since it has an enhanced impact on cell proliferation, attachment, and differentiation [4,5]. Furthermore, CH hydrogels have been commonly used in various medical applications, including 3D printing, drug delivery, and wound healing, due to their favourable biological and structural properties [6,7]. Some of the problems with the wound dressings on the market recently is that the desired mechanical, chemical, biocompatibility and biodegradability properties cannot be achieved depending on the polymer used [8]. For example wound dressings made from raw chitosan has poor mechanical properties. [9]. Nevertheless, due to CH's weak mechanical properties and bacterial adhesion, the latest studies have shown that pure CH is not enough to be used as a wound-dressing agent [10]. Thus, to overcome these limitations, either different nanostructures such as graphene, carbon nanotubes, and metal nanoparticles (Ag, Au, Zn, etc.) are added to CH, or CH itself is combined with other hydrogels that can efficiently overcome its limitations [11]. On the other hand, biodegradability is also very fundamental property in the wound dressing market. Traditional wound dressings such as cotton wool or lint

* Corresponding author.
** Coreespondence author to: O. Gunduz, Department of Metallurgy and Materials Engineering, Faculty of Technology, Marmara University, Istanbul, Turkey.
E-mail addresses: d.kalaskar@ucl.ac.uk (D. Kalaskar), ucemogu@ucl.ac.uk (O. Gunduz).

https://doi.org/10.1016/j.ijbiomac.2022.05.158
Received 18 March 2022; Received in revised form 9 May 2022; Accepted 22 May 2022
Available online 29 May 2022

Table 1
Experimental groups.

3D-printed patches	CH content (wt%)	XG content (wt%)	Solvents (formic acid/ distilled water)
CH4	4	0	1.5/8.5
CH4/XG(0.25)	4	0.25	1.5/8.5
CH4/XG(0.50)	4	0.5	1.5/8.5
CH4/XG(0.75)	4	0.75	1.5/8.5
CH4/XG(1)	4	1	1.5/8.5
CH4/XG(2)	4	2	1.5/8.5

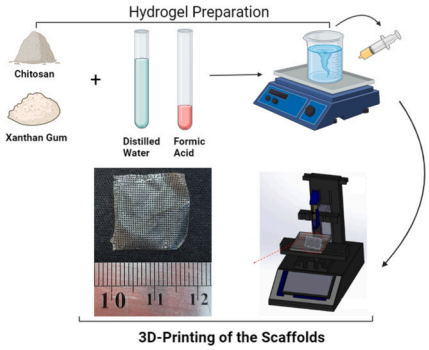

Fig. 1. Schematic representation Of CH-XG patch production.

Table 2
Physical properties of solutions.

Solutions	Density (g/cm^3)	Surface tension (mN/m)	Viscosity (mPa·s)
CH4	1.05	58 ± 0.5	36.29
CH4/XG(0.25)	1.04	62.76 ± 0.8	16.79
CH4/XG(0.50)	1.06	65.3 ± 1.3	21.31
CH4/XG(0.75)	1.10	82.7 ± 2.7	35.6252
CH4/XG(1)	1.15	120.05 ± 0.5	70.02
CH4/XG(2)	1.27	250.15 ± 0.4	300.522

has low degrees of absorbency and low biodegradability that cause incomplete tissue growth after removal [12]. Biodegradable wound dressings are more desirable because of they induce wound healing faster without causing any other injuries. Up to date in modern medicine, desired wound dressings depending on the area has been researched and produced rapidly because of their favourable properties. Xanthan gum (XG) is a microbial *exo*-polysaccharide with numerous advantages, including excellent biocompatibility, biodegradability, non-toxicity, intrinsic ability as an immunological agent, and good quality water solubility [13]. Recently XG has been researched mostly because of its effects on printability, and the results show us that desired printability values can be obtained by blending it with other polymers [46]. Also, in the literature, XG was blended with GelMA to produce wound dressings because of its excellent printability and swelling performance [14]. XG and XG-based biomaterials exhibit high rheological properties such as forming a highly viscous solution at low shear forces, high pseudo-plasticity, and a high viscosity yield value [15]. Besides, XG is widely known for the appropriate redevelopment of damaged tissues and has been explored in various biomedical and tissue engineering applications [13]. In addition, previous studies have shown that the hydrogel prepared by the combination of XG with another polysaccharide, such as CH, exhibited great biocompatibility analysis under in vitro and in vivo models with fibroblast cell line L-929 [16]. Ideal hydrogel for 3D-Printing should have sufficiently high strength, with proper viscosity, and could be printable below the extrusion pressure of the printer and still capable of fusing with earlier printed layers while keeping the print shape [17]. That's why we used CH-XG hydrogel to meet these requirements. 3D printable hydrogels based on biocompatible natural polymers, gelatin, and xanthan gum at different percentages are being used both as scaffolds for cell growth and wound dressing. These latest experiments showed that gelatin/xanthan-gum bioprinted hydrogels are biocompatible materials, as they allowed both human keratinocyte and fibroblast in vitro growth [18]. 3D printing technology has been used in many types of research lately in order to mimic organs or treat the damaged tissue by producing wound dressings. Many types of natural polymers can be used in this field, and even the dressings can be reinforced with materials such as carbon nanofibers [19]. The reason for using 3D printing technology in this research is that it has high reproductivity, precise control during the printing process, and availability in tissue engineering [20]. Also 3D printing technology allows us adaptability and repeatability that can overcome the lacking properties of conventional biofabrication techniques [21]. Although numerous previous studies have reported using CH-based bioinks to produce biodegradable films or electrospun patches, most used CH with other polymers such as polylactide and XG due to its poor mechanical properties [22,23]. However, the extrusion 3D bioprinting of CH-XG blends has not been reported yet. This study is aimed to produce an optimised composition of CH-XG for bioprinting applications, focusing on tailed mechanical, thermal and biocompatible properties for wound healing applications. In this study, we successfully performed 3D printing of CH-XG patches. Finally, we compared 3D printed CH-XG patches with raw 3D printed CH patches and proved the advantages of the 3D printed CH-XG patches based on the mechanical, thermal, biocompatible and high cell proliferation properties. We believe that 3D printed CH-XG patches will be a new perspective in further studies about tissue engineering.

2. Materials and methods

2.1. Materials

Xanthan gum (CAS NO.: 11138-66-22, molecular weight 933.7462 g/mol) and chitosan (CAS NO.: 9012-76-4, particle size 80 Mesh) and sodium hydroxide(NaOH) were purchased from Yasin Teknik Company. Formic acid (HCOOH) and acetic acid (CH_3COOH) were purchased from Merck Co.

2.2. Preparation and characterization of CH/XG hydrogels

Several CH solutions with different Xanthan gum ratios were prepared, as shown in Table 1. CH and XG were dissolved by adding 20 mL of 15% aqueous formic acid solution. Then, the answers were mixed with a magnetic stirrer (Wise Stir®, MSH-20 A, Germany) at 350 rpm for about 24 h. at 90 °C. The density and surface tension of the solutions were measured. Also, viscosity-stress-shear rate and loss modulus-storage modulus were analysed depending on the temperature values. These rheological experiments were determined using a TA Instruments DHR-3, USA instrument using cone plate geometry at 25 °C with 1000 gap value, 2.5 cm parallel plate. The measurement parameters were 1–100 s-1 shear rate, 1 Hz frequency, and %1 strain for the shear rate/stress scanning. Also, for temperature ramp experiment, 1 Hz frequency, %1 strain was applied, and temperature was decreased from 37 °C to 15 °C at 2 °C/min.

Density was measured using a 10 ml pycnometer. All the experiments were performed at room temperature (23 °C).

2.3. 3D printing of the CH/XG patches

The patch configuration was designed in a 20 mm × 20 mm square using Solidworks 2020 program and then converted to G-codes. The prepared polymer solutions were taken into a syringe that had 0.2 mm diameter needle. Then a total of 8 layers were printed with an extrusion-based 3D printer (Hyrel 3D, SDS-5 Extruder, GA, USA). The flow rate was set to 1 ml/h, and printing speed was 10 mm/s [24]. After this

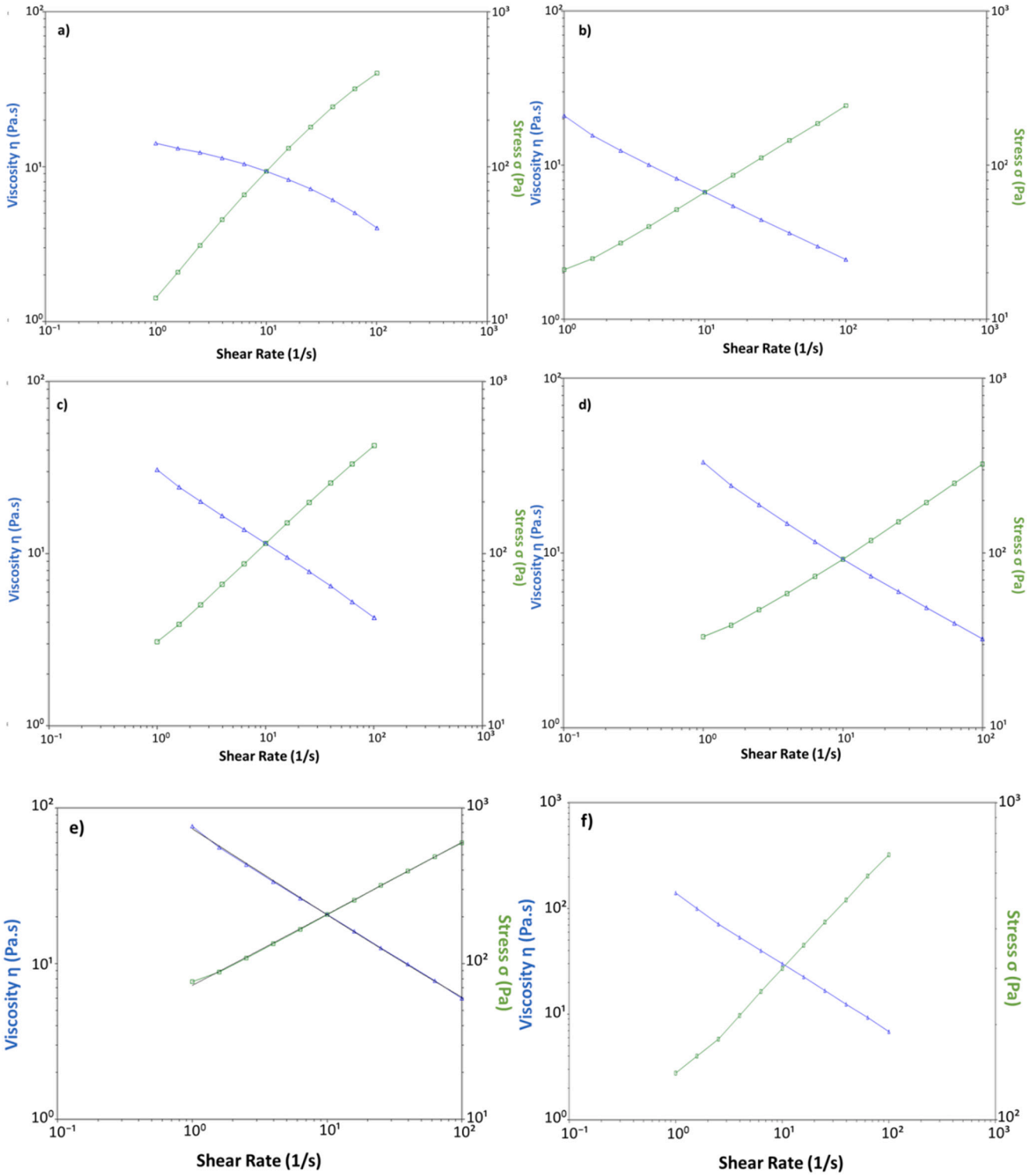

Fig. 2. Viscosity-stress-shear rate graphs of the CH4 (a), CH4/XG(0.25) (b), CH4/XG(0.50) (c), CH4/XG(0.75) (d), CH4/XG(1) (e), CH4/XG(2) (f) solutions.

process, 3D printed patches were crosslinked with sodium hydroxide for 3 min. In Fig. 1, CH-XG patch production is shown.

2.4. Physical characterization of 3D-printed patches

The functional groups in the structure of the used biopolymers were determined by applying Fourier Transform-infrared spectrum (FTIR, Jasco, Japan). CH-XG patches, pure CH patches and pure XG powder were examined in all the spectral bands ranging between 400 cm^{-1} and 4000 cm^{-1} wavelengths. For the thermal properties, DSC (Shimadzu, Japan) was used to investigate how the heat capacities of the samples change concerning temperature. Noting that, temperature ranges were set from 25 °C to 300 °C for all 3D printed patches. Besides, the 3D-Printed patches were observed under SEM (EVO LS 10, ZEISS, München, Germany) to study their morphology and microstructure. Moreover, the mechanical properties of the 3D-Printed patches were

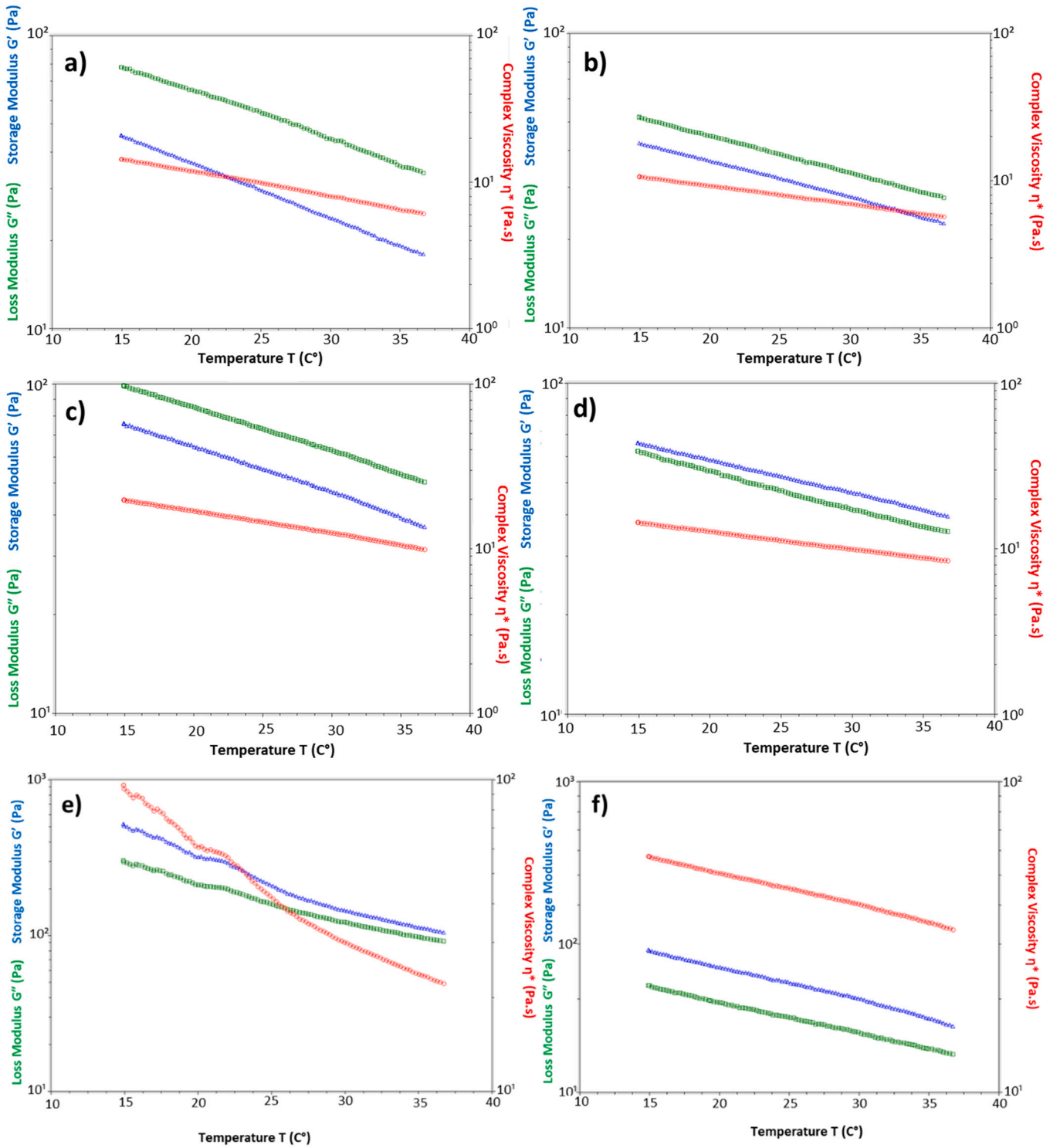

Fig. 3. Temperature dependent loss modulus-storage modulus and complex viscosity graphs of the CH4 (a), CH4/XG(0.25) (b), CH4/XG(0.50) (c), CH4/XG(0.75) (d), CH4/XG(1) (e), CH4/XG(2) (f) solutions.

determined by a tensile test device (Shimadzu EZ-X, Tokyo, Japan) under parameters of 5 kN load, 5 mm/min speed and 0.1 N force applied. Three samples were used from each patch, and as a result, the tensile strength and strain values were obtained. Besides, the initial mass of the samples was weighed to examine the swelling and degradation properties of the patches. For the swelling test, patches were placed in 1 ml of phosphate-buffered saline (PBS), 7.4 pH. Then, the patches were incubated in a thermal shaker at room temperature for 24 h. After that, the mass of each patch was measured by drying it with filter paper at 24-h intervals. Finally, the swelling (S) was measured by applying the following equalisation [25]:

$$S = (Ww - Wd)/Wd \times 100 \quad (1)$$

On the other hand, for the degradation test, the patches were placed in 1 ml of PBS and kept for 24 h, then they were removed from the PBS and dried at 37 degrees in ETUV for 24 h. After that, this process was proceeded periodically every 24 h. Lastly, the degradation value was

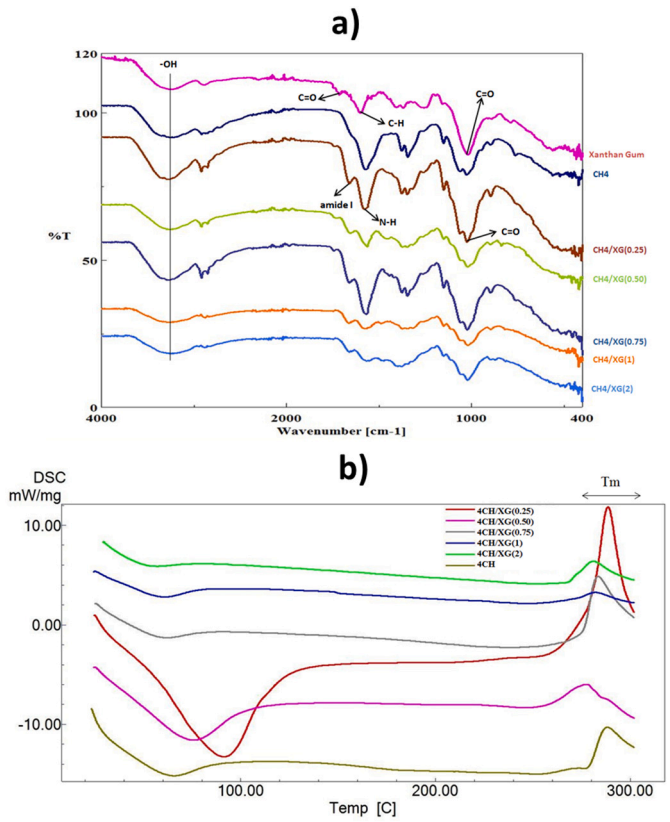

Fig. 4. FTIR Spectra of the Patches(a) and DSC Thermograph(b) of the 3D Printed Patches.

evaluated by using the following equation [25]:

$$Di = (W0 - Wt)/W0 \times 100 \quad (2)$$

To determine the biocompatibility and cell growth properties of the patches, first, they were sterilised under UV for an hour in 96 well plates [26]. The patches were incubated in a growth medium(DMEM with 0.1 mg/ml penicillin/streptomycin and 10% FBS) to optimise the patch microenvironment at 37 °C for an hour in a moist 5% CO_2 incubator. The patches were taken away after the incubation period and the remaining medium was removed using a micropipette. 1×10^4 mouse embryonic fibroblast cells (NIH 3T3) were planted onto the patches in the 96 well plates. Simultaneously, monolayer cell cultures were incubated with the same number of cells in 200 μl to prepare control groups. Then, the cultures were incubated at 37 °C, 5% CO_2 for 1, 4 and 7 days in a humidified incubator. MTT assay was used to determine the cytotoxicity of patches (Vybrant MTT Cell Proliferation Assay Kit, Thermo Fischer Scientific). After the incubation, 10 μL MTT was added to each well to a final concentration of 5 mg/mL and incubated at 37 °C for 4 h. At the end of 4 h, 100 μl of sodium dodecyl sulfate (SDS) was added to the wells and incubated at 37 °C for 12 h to dissolve the formazan crystals formed with MTT. The culture plate was placed on a microplate reader, and the absorbances at wavelengths of 570 and 630 nm were measured by a microplate reader (Biotek, Winooski, VT, USA). Viability was calculated as follows: Cell Viability (%) = (OD test /OD control) × 100. The experiment was done three times.

To examine the attachment and cell viability of fibroblast cells on patches, acridine orange staining was implemented. On days 1, 4 and 7, the growth medium of the cells was removed. And they were scrubbed with PBS. Then, patches were fixed by adding 4% paraformaldehyde at room temperature for 30 min. After that, patches were washed with PBS. Subsequently, 6 μg/ml acridine orange was added to every sample and kept at room temperature for 10 min. Afterwards, the acridine orange solution was discarded and washed three times with PBS.

Then, patches were arranged between the slide and coverslip. The morphology of fibroblast cells on the patches were measured by scanning electron microscope (SEM). The growth medium was rejected after 1, 4 and 7 days. Also all patches were dehydrated through exact dilutions of ethanol and dried in air following the fixation with 4% glutaraldehyde. In order to examination by SEM (EVO MA-10, Zeiss), the samples were sputter-coated with gold.

2.5. Statistical analysis

Pore size measurements were performed using the SPSS 17.0 (IBM, Armonk, NY, USA) analysis program. Data are presented as mean ± SD. For the cell viability test, the level of significance was taken as $p < 0,05$ and the data were labeled with (*) for $p < 0,05$ using One-way Analysis of Variance (ANOVA) Tukey-Kramer Multiple Comparisons Test Comparison to 2D. Also other experiments were performed at least in triplicate.

3. Results and discussion

As shown in Table 2, adding XG to the polymer solution caused a gradual increase in the density, and a rapid increase in the surface tension. XG solutions usually have high density and high viscosity at low concentrations. Therefore, such properties allow XG to be used as a thickening agent [27]. Subsequently, with the increase of the XG concentration, the density is increasing and causing a rapid increase in the surface tension. [28]. In rheology, when the viscosity of a fluid decreases under shear strain, it is evaluated as shear thinning(non-Newtonian) behaviour [28]. It is also called pseudoplastic behaviour. Both preferred materials in this work are shear-thinning polymers [29,30]. Results reported in Fig. 2 is consistent with this information. Where both hydrogel materials followed shear thinning behaviour (pseudoplastic non-Newtonian behaviour).

Furthermore, the shear stress as a function of shear rate curves shows a similar response for all the patches used in this study. The storage modulus gives clues about the structure present in a substance. It displays the energy that is stored in the elastic structure of a sample. If the storage modulus is higher than the loss modulus, it can be said that the material is mainly elastic [31].

Fig. 3 shows that adding more than 0.50% XG to the CH caused hydrogel to show elastic behaviour. Because storage modulus became higher than the loss modulus in these ratios. In Fig. 4(a), CH4 showed two strong vibrations at 1645 cm^{-1} and 1584 cm^{-1}. Furthermore, vibrations of amine deformation generally create very strong bands in the 1638–1575 cm^{-1} area. Therefore, it is suggested that the band at 1583 cm^{-1} represents the N—H bending vibration, whereas the 1645 cm^{-1} band represents the amide I vibration [32].

Fig. 4(a) exhibits the infrared spectra of pure XG, pure CH and CH-XG patches. Besides, the significant peaks for XG at the wavelengths measured in the range of 4000–400 cm^{-1} are: axial deformation of —OH in the 3200–3450 cm^{-1} range; axial deformation of C—H and CHO in the range of 2850–2950 cm^{-1}; axial deformation of C=O ester acid carboxylic, aldehydes and ketones in the range of 1710–1730 cm^{-1}; axial deformation of C=O of enols in the range of 1530–1650 cm^{-1}; reflection angle C—H in the range of 1420–1430 cm^{-1}; and finally, there is an axial deformation of C=O in the range of 1050–1150 cm^{-1} [33]. Additionally, in CH spectrum the carbonyl band was noticed at 1667 cm^{-1} and also the amine (NH2) band at 1590 cm^{-1} [34]. The differential scanning calorimetry (DSC) curves of the 3D printed patches are shown in Fig. 4 (b). Although, the glass transition temperature(*Tg*) of CH is still being researched. In natural polymers, some features such as crystallinity, molecular weight, and deacetylation degree can display wide variations according to the source and method of extraction so that these situations influence the *Tg* [35]. Glass temperature of CH was observed at 30 °C by some researchers for water contents ranging from 8 to 30% [36]. On the

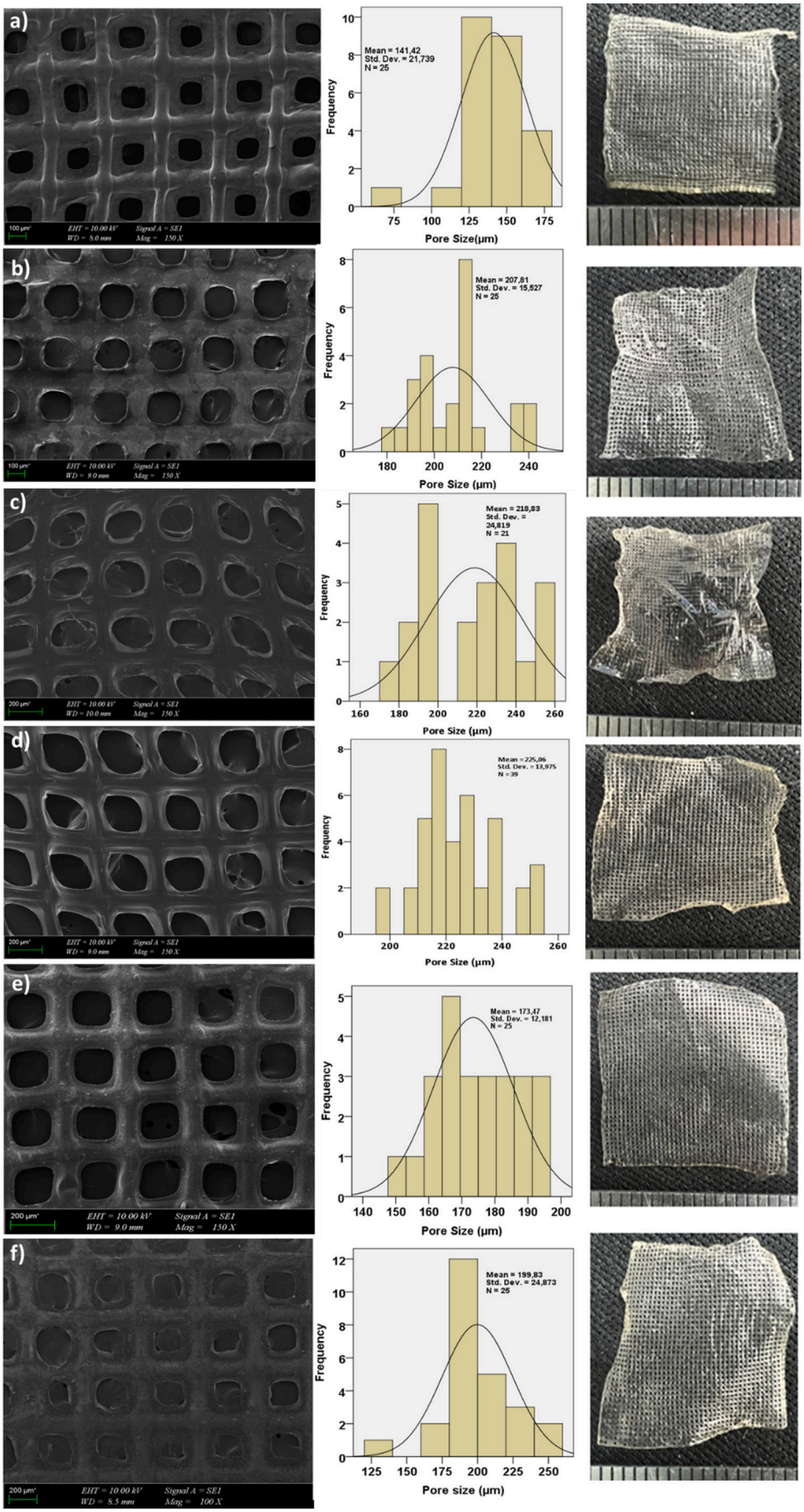

Fig. 5. SEM & Digital Images of the CH4 (a), CH4/XG(0.25) (b), CH4/XG(0.50) (c), CH4/XG(0.75) (d), CH4/XG(1) (e), CH4/XG(2) (f) Patches and Their Pore Size Distributions.

Table 3
Mechanical test results obtained from the tensile test.

3D patches	Tensile strength (MPa)	Strain at break (%)
CH4	2.48 ± 0.54	20.84 ± 2.94
CH4/XG(0.25)	3.38 ± 1.22	13.33 ± 0.69
CH4/XG(0.50)	3.65 ± 0.14	18.02 ± 5.91
CH4/XG(0.75)	3.78 ± 1.25	19.11 ± 2.35
CH4/XG(1)	4.21 ± 2.04	20.81 ± 6.64
CH4/XG(2)	3.10 ± 1.95	8.74 ± 3.68

other hand, other researchers found *Tg* ranging between −23 and 67 °C, depending on the water content, which indicates us in both cases the plasticising effect of water [37].. Furthermore, Sakurai et al. [38] [38] observed the Tg of CH at 203 °C. With the addition of the Xanthan Gum in this study, there were only a few differences between the glass temperatures and melting temperatures of the 3D printed patches, where obtained glass temperatures were around 60 °C–80 °C and obtained melting temperatures were around 280 °C–300 °C. Besides, in Fig. 5, the SEM pictures showed that adding XG to the pure CH increased the pore sizes. This increase is due to the increase in the viscosity after adding XG to the polymer solutions, thus leading to the enlargement of the pores [39].

Regarding the mechanical properties, the tensile testings of all 3D-Printed patches were carried out at room temperature (23 °C). Besides, the tensile strength and strain values just after rupture are presented in Table 3.

Based on the literature, pure CH usually has poor tensile strength, showing a significant decrease in tensile strength at patches with more than 5% CH [40]. Moreover, according to previous studies, adding XG to polymer solutions increases mechanical properties and improves them [41]. Hence, XG was added to the solution in different ratios to improve the poor tensile strength of pure CH. Interestingly, the highest tensile strength was obtained in the 1% XG compared with the other compositions. In research, XG was added to gelatin and carboxymethyl cellulose blends, and there were small decreases than the control group on the tensile strength and also strain at break. [41]. In our research,

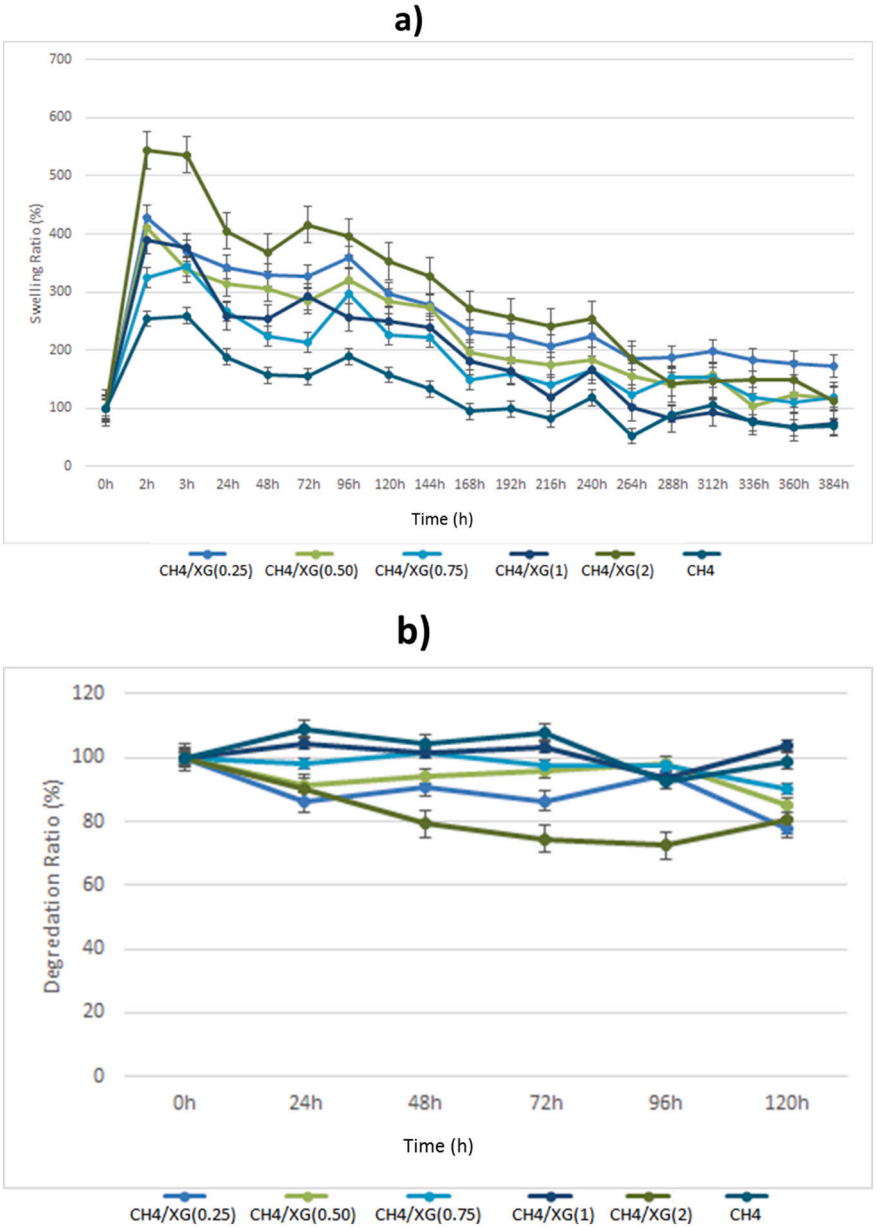

Fig. 6. Swelling kinetics of the 3D printed patches (a), Degradation behaviour of the 3D printed patches (b).

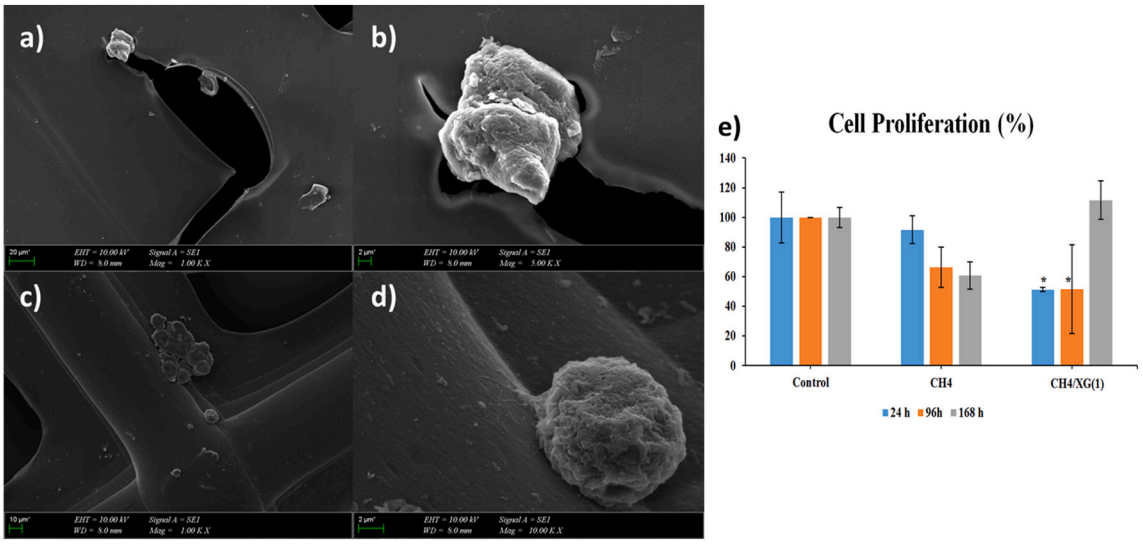

Fig. 7. SEM images of the fibroblast cells on the 3D-printed patches 1 day after the cells are seeded: CH4 1 day (scale bar 20 μm, 1000× magnification) (a), CH4 1 day (scale bar 2 μm, 5000× magnification) (b), CH4/XG(1) 1 day (scale bar 10 μm, 1000× magnification) (c), CH4/XG(1) 1 day (scale bar 2 μm, 10,000× magnification) (d) and Cell viability results of raw CH and CH4/XG(1) patches after 24,96 and 168 h incubation(e).

because of blending it with another polymer and chitosan's poor mechanical properties, these values were increased linearly [40]. Adding the XG into the 4% CH increased the tensile strength and strain values. 1% XG patch showed almost the same strain rupture with pure CH. Adding more than 1% XG to the patches caused a massive drop in strain values. On the other hand, based on the literature, CH has a hydrophilic nature [42]. Hence, increasing the amount of the XG showed us that it can be more hydrophilic. Swelling behaviour is an essential property of hydrogels. In some situations, swelling behaviour can be influenced by external triggers such as pH, ionic strength, and also the temperature of the environment [43]. A desirable wound dressing must create and keep a moist environment while it absorbs the wound fluids besides protecting the wound from infections [44]. Additionally, the water absorption/swelling test was carried out to investigate the effect of XG polymer on the water uptake capacity of the prepared patches.

In Fig. 6(a), the results of the water absorption test of both pure CH and CH-XG patches can be seen in the PBS (pH 7.4) for 384 h at preset time intervals. Gain of weight was calculated, and a graph against time was obtained. The increased XG content in the patches leads to increased water uptake since XG is a more hydrophilic polymer than CH [45]. As Fig. 6(a) shows, the water absorption capacity of the patches with XG/CH is higher than the pure CH patch. Fig. 6(b) shows the degradation percentages of the patches in PBS. Thus, by examining the biodegradability of the patches, it was observed that CH4/XG(1) showed a low degradation rate compared to the other patches. MTT assay was experienced for 1, 4, and 7 days of incubation to determine the cell viability of patches.

The cell viability contents of the patches are shown in Fig. 7(e). At the end of the first day of the experiment, the cell viability value (51.29%) was observed in CH4, and the CH4/XG(1) value was observed (71.29%). On the fourth day, the cell viability was increased by CH4/XG (1) (71.6%, respectively), while it was also increased by CH4 (66.42%, respectively). Cell viability contents were significantly increased for both patches, with the highest value in the CH4/XG(1) on day 7 (162.56%). On the other hand, acridine orange staining confirmed the cell proliferation results. Similarly, it can be seen in Fig. 7(a,b,c,d) that the fibroblast cells in the CH4/XG(1) patch were spread better as compared to the other groups.

4. Conclusions

Novel CH/XG 3D patches were produced using the 3D printing method at different CH/XG ratios. Firstly, the printability of the obtained hydrogels was measured. And the results indicated that printability got better with increasing the XG. Also, the hydrogels showed shear thinning behaviour. Moreover, by adding xanthan gum, the low mechanical properties of pure CH were improved. CH4/XG(1) patches provided excellent physical features such as tensile strength and pore sizes. Adding more than 1% XG to the pure CH caused massive drops in the mechanical properties. The swelling behaviour indicated increased water uptake with increasing XG content in the patches. Consequently, it is expected that this study may have application for skin tissue engineering or dressing for wound healing, considering CH4/XG(1) patches are optimised to be used for that purpose and also can be improved by further studies. Both material optimisation and field characteristics will be considered.

CRediT authorship contribution statement

Eray Altan: Conceptualization, Methodology, Investigation, Writing – original draft. **Nurgul Turker:** Methodology, Investigation, Writing – original draft. **Osama Ali Hindy:** Investigation, Writing – original draft. **Zeynep Dirican:** Investigation. **Ozlem Bingol Ozakpinar:** Investigation. **Aysegul Uzuner Demir:** Investigation. **Deepak Kalaskar:** Writing – original draft. **Sourbh Thakur:** Writing – original draft. **Oguzhan Gunduz:** Methodology, Investigation, Writing – original draft.

References

[1] R.J. Hay, M. Augustin, C.E.M. Griffiths, W. Sterry, The global challenge for skin health, Br. J. Dermatol. 172 (6) (2015) 1469–1472.
[2] D.J. Cornelissen, A. Faulkner-Jones, W. Shu, Current developments in 3D bioprinting for tissue engineering, Curr.Opin.Biomed.Eng. 2 (2017) 76–82.
[3] M.R. Kumar, R. Muzzarelli, C. Muzzarelli, H. Sashiwa, A.J. Domb, Chitosan chemistry and pharmaceutical perspectives, Chem. Rev. 104 (12) (2004) 6017–6084.
[4] A. Di Martino, M. Sittinger, M.V. Risbud, Chitosan: a versatile biopolymer for orthopaedic tissue-engineering, Biomaterials 26 (30) (2005) 5983–5990.
[5] S. Saravanan, R.S. Leena, N. Selvamurugan, Chitosan based biocomposite scaffolds for bone tissue engineering, Int. J. Biol. Macromol. 93 (2016) 1354–1365.
[6] J. Fu, F. Yang, Z. Guo, The chitosan hydrogels: from structure to function, New J. Chem. 42 (21) (2018) 17162–17180.
[7] S. Peers, A. Montembault, C. Ladavière, Chitosan hydrogels for sustained drug delivery, J. Control. Release 326 (2020) 150–163.

[8] K. Valachová, M.A. El Meligy, L. Šoltés, Hyaluronic acid and chitosan-based electrospun wound dressings: problems and solutions, Int. J. Biol. Macromol. 206 (2022) 74–91, https://doi.org/10.1016/j.ijbiomac.2022.02.117.
[9] T.G. Ambaye, M. Vaccari, S. Prasad, E.D. van Hullebusch, S. Rtimi, Preparation and applications of chitosan and cellulose composite materials, J. Environ. Manag. 301 (2022), 113850.
[10] L. Geng, W. Feng, D.W. Hutmacher, Y. San Wong, H.T. Loh, J.Y. Fuh, Direct writing of chitosan scaffolds using a robotic system, Rapid Prototyp. J. 11 (2) (2005) 90–97, https://doi.org/10.1108/13552540510589458.
[11] I.T. Ozbolat, M. Hospodiuk, Current advances and future perspectives in extrusion-based bioprinting, Biomaterials 76 (2016) 321–343.
[12] M. Farokhi, F. Mottaghitalab, Y. Fatahi, A. Khademhosseini, D.L. Kaplan, Overview of silk fibroin use in wound dressings, Trends Biotechnol. 36 (9) (2018) 907–922.
[13] A. Kumar, K.M. Rao, S.S. Han, Application of xanthan gum as polysaccharide in tissue engineering: a review, Carbohydr. Polym. 180 (2018) 128–144.
[14] Z. Yang, X. Ren, Y. Liu, Multifunctional 3D printed porous GelMA/xanthan gum based dressing with biofilm control and wound healing activity, Mater. Sci. Eng. C 131 (2021), 112493.
[15] S. Rosalam, R. England, Review of xanthan gum production from unmodified starches by Xanthomonas comprestris sp, Enzym. Microb. Technol. 39 (2) (2006) 197–207.
[16] F. Chellat, M. Tabrizian, S. Dumitriu, E. Chornet, P. Magny, C.H. Rivard, L. H. Yahia, In vitro and in vivo biocompatibility of chitosan-xanthan polyionic complex, J.Biomed.Mater.Res. 51 (1) (2000) 107–116.
[17] F.C. Godoi, S. Prakash, B.R. Bhandari, 3d printing technologies applied for food design: status and prospects, J. Food Eng. 179 (2016) 44–54.
[18] B. Piola, M. Sabbatini, S. Gino, M. Invernizzi, F. Renò, 3D bioprinting of gelatin-xanthan gum composite hydrogels for growth of human skin cells, Int. J. Mol. Sci. 23 (1) (2022) 539.
[19] A. Serafin, C. Murphy, M.C. Rubio, M.N. Collins, Printable alginate/gelatin hydrogel reinforced with carbon nanofibers as electrically conductive scaffolds for tissue engineering, Mater. Sci. Eng. C 122 (2021), 111927.
[20] P.S. Gungor-Ozkerim, I. Inci, Y.S. Zhang, A. Khademhosseini, M.R. Dokmeci, Bioinks for 3D bioprinting: an overview, Biomaterials science 6 (5) (2018) 915–946.
[21] G. Decante, J.B. Costa, J. Silva-Correia, M.N. Collins, R.L. Reis, J.M. Oliveira, Engineering bioinks for 3D bioprinting, Biofabrication 13 (3) (2021), 032001.
[22] M. De Morais Lima, L.C. Carneiro, D. Bianchini, A.R.G. Dias, E.D.R. Zavareze, C. Prentice, A.D.S. Moreira, Structural, thermal, physical, mechanical, and barrier properties of chitosan films with the addition of xanthan gum, J. Food Sci. 82 (3) (2017) 698–705.
[23] Y. Wan, H. Wu, A. Yu, D. Wen, Biodegradable polylactide/chitosan blend membranes, Biomacromolecules 7 (4) (2006) 1362–1372.
[24] E. Ilhan, S. Ulag, A. Sahin, B.K. Yilmaz, N. Ekren, O. Kilic, O. Gunduz, Fabrication of tissue-engineered tympanic membrane patches using 3D-printing technology, J. Mech. Behav. Biomed. Mater. 114 (2021) 104219.
[25] S.N. Alhosseini, F. Moztarzadeh, M. Mozafari, S. Asgari, M. Dodel, A. Samadikuchaksaraei, N. Jalali, Synthesis and characterisation of electrospun polyvinyl alcohol nanofibrous scaffolds modified by blending with chitosan for neural tissue engineering, Int. J. Nanomedicine 7 (2012) 25.
[26] M. Bentancor, S. Vidal, Programmable and low-cost ultraviolet room disinfection device, HardwareX 4 (2018), e00046.
[27] A. Becker, F. Katzen, A. Pühler, L. Ielpi, Xanthan gum biosynthesis and application: a biochemical/genetic perspective, Appl. Microbiol. Biotechnol. 50 (2) (1998) 145–152.
[28] T.G. Mezger, The Rheology Handbook: For Users of Rotational and Oscillatory Rheometers, Vincentz Network GmbH & Co. KG, Hannover, Germany, 2006.
[29] E.A. El-Hafian, E.S. Elgannoudi, A. Mainal, A.H.B. Yahaya, Characterization of chitosan in acetic acid: rheological and thermal studies, Turk. J. Chem. 34 (1) (2010) 47–56.
[30] L. Zhong, M. Oostrom, M.J. Truex, V.R. Vermeul, J.E. Szecsody, Rheological behaviour of xanthan gum solution related to shear-thinning fluid delivery for subsurface remediation, J. Hazard. Mater. 244 (2013) 160–170.
[31] A. Franck, T.I. Germany, Viscoelasticity and Dynamic Mechanical Testing, TA Instruments, New Castle, DE, USA AN004, 1993.
[32] G. Lawrie, I. Keen, B. Drew, A. Chandler-Temple, L. Rintoul, P. Fredericks, L. Grøndahl, Interactions between alginate and chitosan biopolymers characterized using FTIR and XPS, Biomacromolecules 8 (8) (2007) 2533–2541.
[33] S. Faria, C.L. de Oliveira Petkowicz, S.A.L. De Morais, M.G.H. Terrones, M.M. De Resende, F.P. de Franca, V.L. Cardoso, Characterization of xanthan gum produced from sugar cane broth, Carbohydr. Polym. 86 (2) (2011) 469–476.
[34] Z. Osman, A.K. Arof, FTIR studies of chitosan acetate-based polymer electrolytes, Electrochim. Acta 48 (8) (2003) 993–999.
[35] C.D.T. Neto, J.A. Giacometti, A.E. Job, F.C. Ferreira, J.L.C. Fonseca, M.R. Pereira, Thermal analysis of chitosan-based networks, Carbohydr. Polym. 62 (2) (2005) 97–103.
[36] J. Ratto, T. Hatakeyama, R.B. Blumstein, Differential scanning calorimetry investigation of phase transitions in water/chitosan systems, Polymer 36 (15) (1995) 2915–2919.
[37] A. Lazaridou, C.G. Biliaderis, Thermophysical properties of chitosan, chitosan–starch and chitosan–pullulan films near the glass transition, Carbohydr. Polym. 48 (2) (2002) 179–190.
[38] K. Sakurai, T. Maegawa, T. Takahashi, Glass transition temperature of chitosan and miscibility of chitosan/poly (N-vinyl pyrrolidone) blends, Polymer 41 (19) (2000) 7051–7056.
[39] J.L. Zatz, S. Knapp, Viscosity of xanthan gum solutions at low shear rates, J. Pharm. Sci. 73 (4) (1984) 468–471.
[40] S.A.B.M. Isa, R. Mohammed, Physical and mechanical properties of chitosan and polyethylene blend for food packaging film, Int.J.Mech.Prod.Eng. 3 (10) (2015) 51–55.
[41] M.N. Hazirah, M.I.N. Isa, N.M. Sarbon, Effect of xanthan gum on the physical and mechanical properties of gelatin-carboxymethyl cellulose film blends, Food Packag. Shelf Life 9 (2016) 55–63.
[42] F. Ahmadi, Z. Oveisi, S.M. Samani, Z. Amoozgar, Chitosan-based hydrogels: characteristics and pharmaceutical applications, Res.Pharm.Sci. 10 (1) (2015) 1.
[43] X. Lin, Q. Ma, J. Su, C. Wang, R.K. Kankala, M. Zeng, S.F. Zhou, Dual-responsive alginate hydrogels for controlled release of therapeutics, Molecules 24 (11) (2019) 2089.
[44] M. Kokabi, M. Sirousazar, Z.M. Hassan, PVA–clay nanocomposite hydrogels for wound dressing, Eur. Polym. J. 43 (3) (2007) 773–781.
[45] R. Kar, S. Mohapatra, S. Bhanja, D. Das, B. Barik, Formulation and in vitro characterization of xanthan gum-based sustained release matrix tables of isosorbide-5-mononitrate, Iran.J.Pharm.Res. 9 (1) (2010) 13.
[46] P. García-Segovia, V. García-Alcaraz, S. Balasch-Parisi, J. Martínez-Monzó, 3D printing of gels based on xanthan/konjac gums, Innovative Food Sci. Emerg. Technol. 64 (2020), 102343.